ISEV

Engineered small extracellular vesicles displaying ACE2 variants on the surface protect against SARS-CoV-2 infection

Hark Kyun Kim[1] | Junhyung Cho[2] | Eunae Kim[1] | Junsik Kim[1] | Jeong-Sun Yang[2] | Kyung-Chang Kim[2] | Joo-Yeon Lee[2] | Younmin Shin[2] | Leon F. Palomera[1] | Jinsu Park[1] | Seung Hyun Baek[1] | Han-Gyu Bae[1] | Yoonsuk Cho[1] | Jihoon Han[1] | Jae Hoon Sul[1] | Jeongmi Lee[1] | Jae Hyung Park[3,4,5,7] | Yong Woo Cho[6,7] | Wonsik Lee[1] | Dong-Gyu Jo[1,3,4,7] (iD)

[1] School of Pharmacy, Sungkyunkwan University, Suwon, Republic of Korea

[2] Division of Emerging Viral Diseases and Vector Research, Centre for Infectious Diseases Research, Korea National Institute of Health, Korea Centres for Disease Control and Prevention Agency, Cheongju, Republic of Korea

[3] Biomedical Institute for Convergence, Sungkyunkwan University, Suwon, Republic of Korea

[4] Department of Health Sciences and Technology, Samsung Advanced Institute for Health Sciences & Technology (SAIHST), Sungkyunkwan University, Seoul, Republic of Korea

[5] School of Chemical Engineering, Sungkyunkwan University, Suwon, Republic of Korea

[6] Department of Materials Science and Chemical Engineering, Hanyang University ERICA, Ansan, Republic of Korea

[7] ExoStemTech Inc., Ansan, Republic of Korea

Correspondence
Dong-Gyu Jo and Wonsik Lee, School of Pharmacy, Sungkyunkwan University, Suwon, Republic of Korea.
Email: jodg@skku.edu and wonsik.lee@skku.edu

Hark Kyun Kim and Junhyung Cho contributed equally.

Funding information
the National Research Foundation of Korea, Grant/Award Numbers: NRF-2019R1A2C3011422, NRF-2019R1A5A2027340; the Ministry of Oceans and Fisheries' R&D project, Korea, Grant/Award Number: 1525011845; Korea Basic Science Institute (National Research Facilities and Equipment Center); the Ministry of Education, Grant/Award Number: 2020R1A6C101A191; Korea Disease Control and Prevention Agency, Grant/Award Number: KCDC 2021-ER1602-00; the Korea National Institute of Health fund, Grant/Award Number: 2021-NI-026-00

Abstract

Severe acute respiratory syndrome coronavirus 2 (SARS-CoV-2) entry is mediated by the interaction of the viral spike (S) protein with angiotensin-converting enzyme 2 (ACE2) on the host cell surface. Although a clinical trial testing soluble ACE2 (sACE2) for COVID-19 is currently ongoing, our understanding of the delivery of sACE2 via small extracellular vesicles (sEVs) is still rudimentary. With excellent biocompatibility allowing for the effective delivery of molecular cargos, sEVs are broadly studied as nanoscale protein carriers. In order to exploit the potential of sEVs, we design truncated CD9 scaffolds to display sACE2 on the sEV surface as a decoy receptor for the S protein of SARS-CoV-2. Moreover, to enhance the sACE2-S binding interaction, we employ sACE2 variants. sACE2-loaded sEVs exhibit typical sEVs characteristics and bind to the S protein. Furthermore, engineered sEVs inhibit the entry of wild-type (WT), the globally dominant D614G variant, Beta (K417N-E484K-N501Y) variant, and Delta (L452R-T478K-D614G) variant SARS-CoV-2 pseudovirus, and protect against authentic SARS-CoV-2 and Delta variant infection. Of note, sACE2 variants harbouring sEVs show superior antiviral efficacy than WT sACE2 loaded sEVs. Therapeutic efficacy of the engineered sEVs against SARS-CoV-2 challenge was confirmed using K18-hACE2 mice. The current findings provide opportunities for the development of new sEVs-based antiviral therapeutics.

KEYWORDS
beta variant, COVID-19, delta variant, extracellular vesicles, SARS-CoV-2, soluble ACE2, spike

1 | INTRODUCTION

At the end of 2019, severe acute respiratory syndrome coronavirus 2 (SARS-CoV-2) emerged as a novel coronavirus, which spread rapidly, causing a pandemic with over a million deaths worldwide (Wu et al., 2020). The subsequent evolution of vaccine-resistant SARS-CoV-2 variants complicated prophylaxis (Madhi et al., 2021). SARS-CoV-2 harbouring S glycoprotein substitution D614G became the most dominant variant and was reported to exhibit greater infectivity (Plante et al., 2021). Further, pseudoviruses of the B1.351 lineage, also known as Beta variant, containing S protein receptor-binding domain (RBD) mutations, including N501Y, E484K, and K417N, exhibited increased resistance to neutralization by therapeutic monoclonal antibodies and convalescent plasma (Wibmer et al., 2021). Delta variant, rapidly sweeping the globe, also showed decreased sensitivity to sera from vaccinated individuals and convalescent individuals (Planas et al., 2021).

ACE2 is one of the main receptors utilized by SARS-CoV-2 for entry into host cells (Hoffmann et al., 2020). The surface S protein on the viral surface binds to the peptidase domain of ACE2 (Wrapp et al., 2020). It has been reported that human recombinant sACE2 can inhibit SARS-CoV-2 infection in kidney organoids, incentivizing further evaluation in clinical trials (Monteil et al., 2020; Zoufaly et al., 2020). To overcome the short half-life of ACE2, a conjugated protein consisting of sACE2 fused with the Fc region of IgG1 exhibited protection against infection with a S protein-harbouring pseudovirus (Lei et al., 2020).

sEVs, 50–200 nm in diameter, include exosomes and microvesicles (Kourembanas, 2015). They can transfer diverse cargos, including proteins, lipids, and various RNAs, facilitating cell-to-cell communication. sEVs have been increasingly exploited as vehicles for the delivery of therapeutic cargos (Yim et al., 2016). CD9 is one of the essential exosomal surface proteins and belongs to the tetraspanin superfamily, having four transmembrane regions and two extracellular loops (Boucheix et al., 1991). Furthermore, CD9 overexpression was shown to enhance the production rate of sEVs (Böker et al., 2018).

Herein, we employed sEVs as carriers of sACE2 and its variants in order to neutralize the S protein of SARS-CoV-2 as an extracellular decoy. To display active sACE2 on the sEVs surface, we utilized CD9 as a scaffold. Moreover, we deleted transmembrane region 4, generating a truncated form of CD9 (CD9ΔTM4). The C terminus end of CD9ΔTM4 was then conjugated with sACE2 in order to present functional sACE2 on the surface of sEVs (CD9ΔTM4-sACE2). Utilizing deep mutagenesis, Chan et al. previously reported mutations in ACE2, which enhanced binding to the viral S protein (Chan et al., 2020). Based on these observations, we used mutated forms of sACE2 with higher binding affinity for the S protein. The engineered sEVs displaying sACE2 inhibited interactions of S with ACE2, and neutralized pseudovirus, authentic wildtype and Delta variant SARS-CoV-2 entry (Figure 1).

2 | RESULTS

2.1 | sEVs targeting strategies and characterization of engineered sEVs

To demonstrate whether the CD9ΔTM4-sACE2(WT) construct could facilitate sACE2 plasma membrane expression, we designed a plasmid encoding eGFP-CD9ΔTM4-sACE2(WT). HEK293T cells were transfected with an empty vector, CD9ΔTM4-sACE2(WT), or eGFP-CD9ΔTM4-sACE2(WT), respectively. Consistent with the previously reported subcellular localization of tetraspanin proteins, cells transfected with eGFP-CD9ΔTM4-sACE2(WT) exhibited cytosolic puncta and membrane localization (Figure S1a, Supporting Information) (Duong et al., 2019). To test whether these fusion proteins could be packaged into sEVs, conditioned media was obtained, centrifuged, filtered, and concentrated by tangential flow filtration (TFF). As controls, sEVs were produced using conditioned media harvested from HEK293T cells (HEK sEVs) and from HEK293T cells expressing CD9ΔTM4-sACE2(WT) (sACE2(WT) sEVs). GFP fluorescence was detected in sEVs containing eGFP-CD9ΔTM4-sACE2(WT) protein, but not in HEK sEVs and sACE2(WT) sEVs (Figure S1b, Supporting Information). To evaluate the loading efficiency of CD9ΔTM4 to sEVs, we isolated sEVs from HEK293T cells expressing human full-length ACE2 (fACE2 sEVs). When compared to fACE2 sEVs, sACE2(WT) sEVs showed significantly higher concentration of sACE2 proteins (Figure S1c, Supporting Information). Western blot for Flag-tagged to ACE2 confirmed these observations (Figure S1d, Supporting Information). Collectively, these results suggest that the overexpression of CD9ΔTM4 scaffolds results in abundant packaging of the fusion protein into sEVs.

To assess the functionality of sEVs membrane sACE2, we utilized CD9ΔTM4-sACE2(WT) scaffolds. Several ACE2 variants were reported in a recent study, two of which were introduced herein (Chan et al., 2020). We assessed the neutralization efficacy of engineered sEVs expressing sACE2.v1 with H34A, T92Q, Q325P, and A386L, as well as sACE2.v2 containing T27Y, L79T, N330Y, and A386L. HEK293T cells were transiently transfected with vectors encoding CD9ΔTM4-sACE2(WT)-3xFlag, CD9ΔTM4-sACE2.v1-3xFlag or CD9ΔTM4-sACE2.v2-3xFlag, and conditioned medium was collected. Three types of sEVs were purified by TFF (sACE2(WT) sEVs, sACE2.v1 sEVs, and sACE2.v2 sEVs). These were characterized according to the MISEV2018 (Minimal Information for Studies of Extracellular Vesicles 2018) guidelines (Théry et al., 2018). As expected, the four different kinds of sEVs had similar spherical morphology and size under cryo-transmission electron microscopy (Cryo-TEM) (Figure 2a). Nanoparticle tracking analysis was performed to quantitate the number of sEVs particles and their size. All sEVs were within the normal vesicle
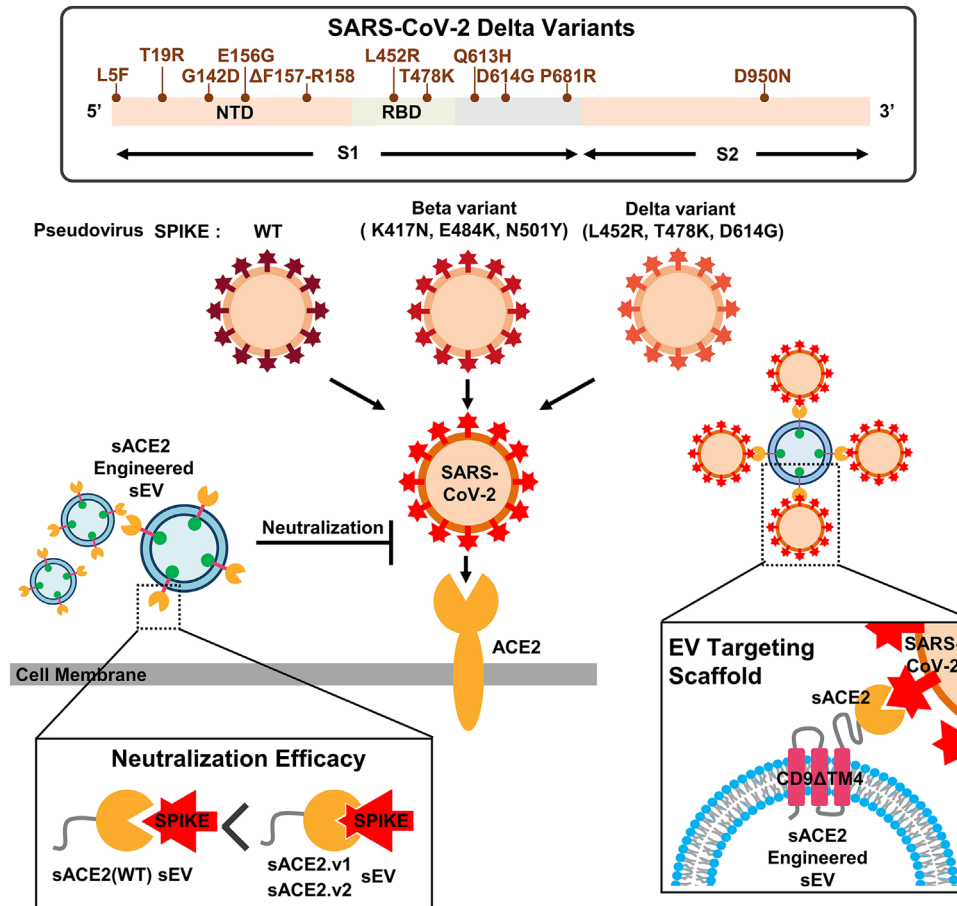
FIGURE 1 Schematic illustration of SARS-CoV-2 infection and the application of engineered sEVs for the neutralization of SARS-CoV-2. Mechanism of engineered sACE2 sEVs targeting the S protein of SARS-CoV-2 by exploiting the affinity of sACE2 for S. The resulting sEVs may represent an sEVs-based antiviral therapy for blocking SARS-CoV-2 infection

size range (50–200 nm) (Figure 2b). Micro BCA assays were performed to determine sEVs protein concentration. The purity of sEVs was assessed based on the number of particles and sEVs protein concentrations (HEK sEVs: 2.72×10^8 particles/μg, sACE2(WT) sEVs: 1.58×10^8 particles/μg, sACE2.v1 sEVs: 4.47×10^8 particles/μg, sACE2.v2 sEVs: 2.72×10^8 particles/μg), indicating that sACE2 overexpression did not alter sEVs purity. Immunoblot analysis of sEVs revealed that sEVs markers ALIX, TSG101, CD9, and CD63 were detected in both cellular lysates and sEVs fractions, whereas CANX and GM130 were only detected in the former, indicative of high-purity sEVs. The presence of ACE2 and Flag in purified sEVs confirmed that overexpressed ACE2 and Flag were efficiently packaged into sEVs (Figure 2c). To analyse surface marker proteins of sEVs, sEVs were incubated with magnetic beads coated with anti-CD63 antibody and then detected with anti-CD81 antibody. The signals for CD81 on all sEVs were confirmed using confocal microscopy and FACS analysis (Figure 2d,e). sACE2 levels in purified sEVs were determined via sACE2 ELISA. sACE2(WT) sEVs, sACE2.v1 sEVs and sACE2.v2 sEVs exhibited significantly higher sACE2 concentrations compared to HEK sEVs (Figure 2f).

2.2 | Binding properties of engineered sACE2 sEVs

In order to compare the binding affinities of sEVs to the S protein, we performed an ACE2: S protein inhibitor screening assay (Figure 3a). S protein preincubated with sACE2(WT) sEVs exhibited a significant dose-dependent reduction in ACE2 interaction. Incubation with sACE2.v1 sEVs and sACE2.v2 sEVs also led to a dramatic dose-dependent decrease in binding affinity compared to either HEK sEVs or sACE2(WT) sEVs, whereas HEK sEVs had no impact on the interaction between S and ACE2 (Figure 3b). These findings were further substantiated via immunoprecipitation (IP) assays. To determine the interaction between sEVs and the S protein under conditions closer to the physiological, we transfected HEK293T cells with an expression vector containing S-TagBFP or an empty control vector. Lysates of transfected HEK293T cells were immunoprecipitated using TagBFP antibody. Magnetic bead-bound S proteins were incubated with sEVs before elution using sample buffer (Figure 3c). The IP assay revealed a
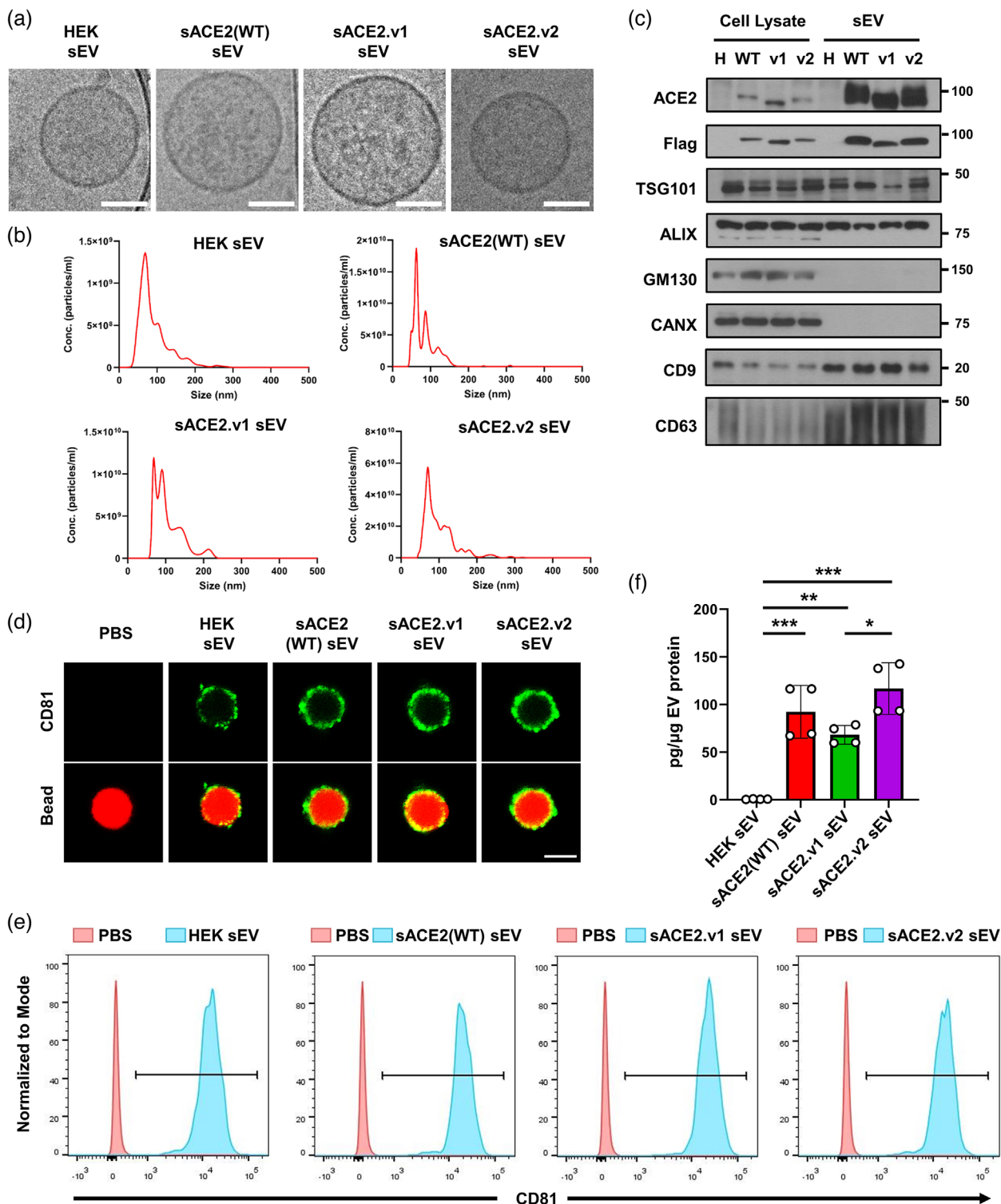
FIGURE 2 Characterization of engineered sACE2 sEVs. (a) Cryo-TEM images of HEK sEVs, sACE2(WT) sEVs, sACE2.v1 sEVs, and sACE2.v2 sEVs. (b) Size distribution of the engineered sEVs was measured using an nanoparticle tracking analysis. (c) Representative western blot analysis of cell lysates and sEVs for ACE2, Flag, TSG101, CANX, GM130, CD9, CD63 and ALIX. H: HEK sEVs, WT: sACE2(WT) sEVs, v1: sACE2.v1 sEVs, v2: sACE2.v2 sEVs. (d) CD81 staining of sEVs and fluorescence images of magnetic beads. (e) Flow cytometry of CD81 expression on sEVs. (f) sACE2 protein concentration in sEVs as determined via ELISA ($n = 4$). Scale bars, 50 nm. Data are presented as the mean $\pm$ s.d. *$P < 0.05$; **$P < 0.01$; ***$P < 0.001$ (one-way ANOVA with Tukey's multiple comparisons test)
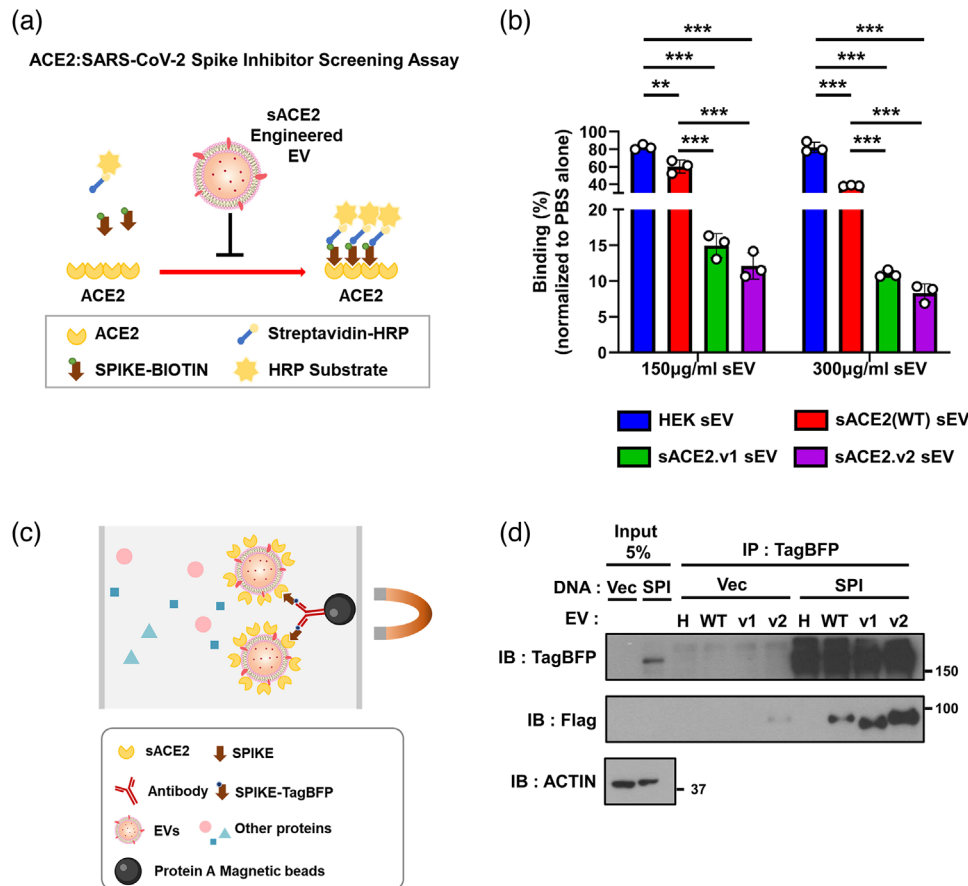
FIGURE 3 Binding properties of engineered sEVs. (a) Scheme of ACE2 : SARS-CoV-2 S inhibitor assay. (b) The effect of HEK sEVs, sACE2(WT) sEVs, sACE2.v1 sEVs, and sACE2.v2 sEVs on the ACE2-S interaction ($n = 3$). (c) Schematic illustration of the immunoprecipitation-based binding assay of sEVs and the S protein. (d) S-TagBFP protein immunoprecipitated from HEK293T cells transfected with the pCMV14 vector (Vec) and pCMV14-SPIKE-TagBFP (SPI) was detected with a TagBFP antibody. sEVs interacting with S-TagBFP were detected using a Flag antibody. H: HEK sEVs, WT: sACE2(WT) sEVs, v1: sAJ. H. Sul, J. M. Jung, J. H. Park, Ji S Choi, Y. W. Cho, D. ?. G. JoCE2.v1 sEVs, v2: sACE2.v2 sEVs. Actin was used as a loading control for immunoblotting. Data are presented as the mean ± s.d. **$P < 0.01$; ***$P < 0.001$ (one-way ANOVA with Tukey's multiple comparisons test **d**)

clear interaction between S and sACE2(WT) sEVs, sACE2.v1 sEVs and sACE2.v2 sEVs in contrast to with HEK sEVs. Consistent with ACE2:S protein binding assay results, sACE2.v1 sEVs and sACE2.v2 sEVs had a superior affinity for the S protein (Figure 3d). Taken together, these results demonstrated that all sACE2-loaded sEVs could bind to the S protein, and sEVs displaying sACE2 variants exhibited more significant increases in S protein binding than sACE2(WT) sEVs.

2.3 | sACE2 sEVs protects against WT and variants of S-containing pseudovirus infection

We then sought to determine whether sACE2 sEVs had the capacity to neutralize SARS-CoV-2 pseudovirus bearing the viral envelope S protein. To test pseudovirus infectivity, HEK293T cells stably expressing human ACE2-TagBFP (HEK293T-hACE2-TagBFP) were generated, and human ACE2 as well as TagBFP expression were confirmed via western blot and flow cytometry (Figure S2a,b, Supporting Information). sACE2.v1 sEVs and sACE2.v2 sEVs potently neutralized pseudovirus infection in HEK293T-hACE2-TagBFP at all tested concentrations, whereas sACE2(WT) sEVs significantly reduced infectivity only at a concentration of 100 and 200 μg/ml (Figure 4a,b). Accumulated continuous mutations in the S protein make SARS-CoV-2 resistant to therapeutic monoclonal antibodies and vaccine-induced neutralizing antibodies (Hu et al., 2021). To test whether S mutations confer resistance against sACE2-loaded sEVs, we generated SARS-CoV-2 pseudovirus containing D614G mutant, RBD mutations in Beta variant-K417N, E484K, and N501Y, and mutations in Delta variant L452R, E484K, and D614G (Figure S3a, Supporting Information). Notably, sACE2.v1 sEVs and sACE2.v2 sEVs blocked D614G mutant infection in a concentration-dependent manner and exhibited 95% inhibition even at 100 μg/ml, which is equivalent to 4.47×10^{10} particles/ml containing 6.82 ng/ml of ACE2 and 2.72×10^{10} particles/ml with 11.68 ng/ml of ACE2, respectively. sACE2(WT) sEVs had marginal effects on the infectivity of D614G mutant pseudovirus compared with that by sACE2.v1 sEVs and sACE2.v2 sEVs (Figure 4c,d). sEVs were
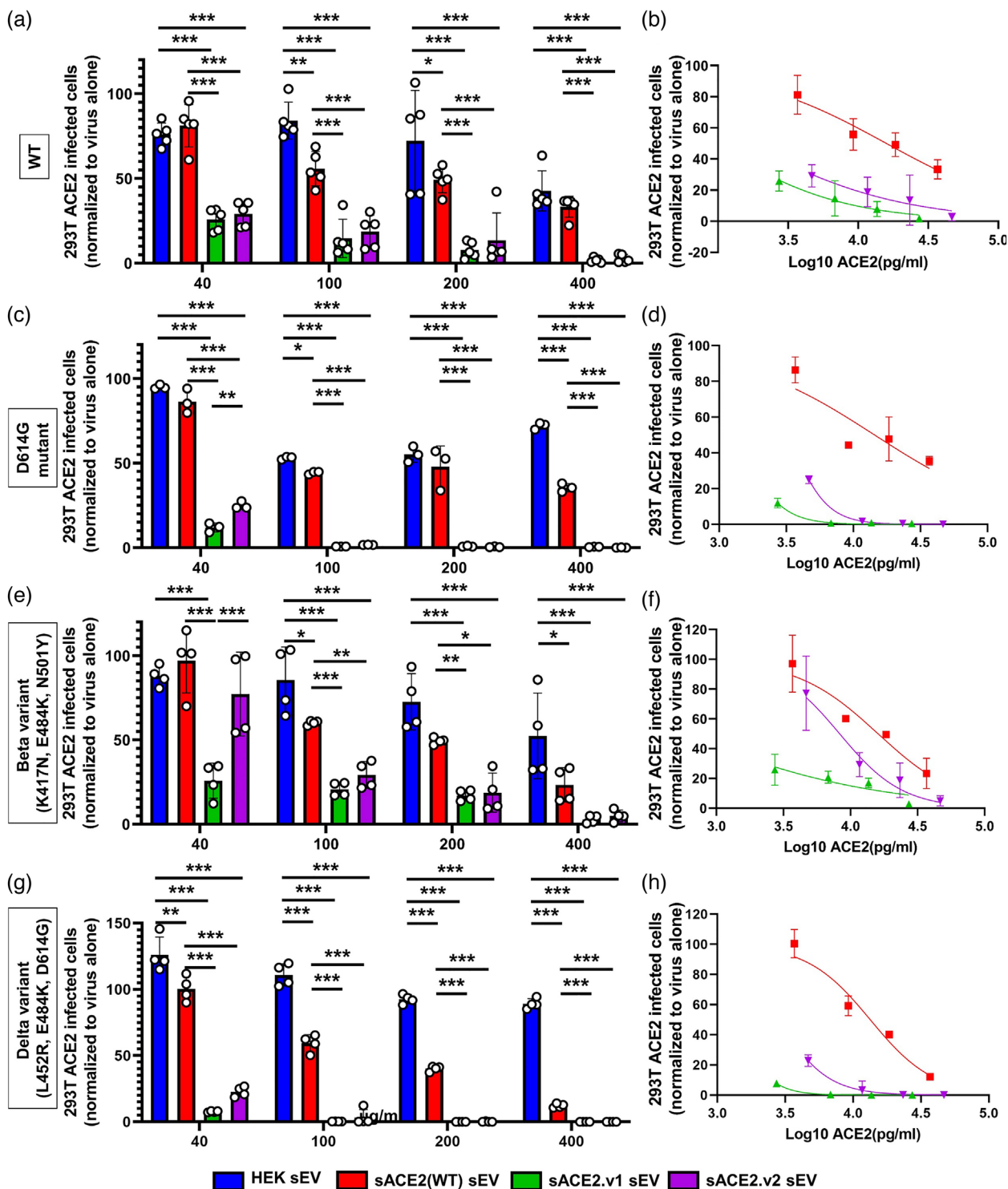
FIGURE 4 Protection against WT and mutant S-containing pseudovirus. (a) Assessment of luciferase-based WT S-containing pseudovirus infectivity in HEK293T-ACE2-TagBFP cells in the presence of sEVs ($n = 5$). Values are normalized to virus alone (100%). (b) WT S-containing pseudovirus infectivity related to the concentration of sACE2 in sEVs evaluated in Figure 2f. (c,d) Infectivity of pseudovirus bearing D614G S proteins ($n = 3$). (e,f) Infectivity of pseudovirus bearing Beta variant S (K417N, E484K, N501Y) proteins ($n = 4$). (g,h) Infectivity of pseudovirus bearing Delta variant S (L452R, E484K, D614G) proteins ($n = 4$). Data are presented as the mean ± s.d. *$P < 0.05$; **$P < 0.01$; ***$P < 0.001$ (one-way ANOVA with Tukey's multiple comparisons test)

also tested against Beta variant pseudovirus. We observed highly efficient Beta variant pseudovirus neutralization by sACE2.v1 sEVs and sACE2.v2 sEVs. sACE2.v1 sEVs blocked Beta variant pseudovirus infection in a concentration-dependent manner and exhibited more 65% inhibition at a concentration of 40 μg/ml (Figure 4e,f). We also characterized the potency of these sEVs against Delta variant pseudovirus. All engineered sEVs markedly neutralize Delta variant pseudovirus in a concentration-dependent manner. Especially, sACE2.v1 sEVs exhibited 92% inhibition even at 40 μg/ml (Figure 4g,h). To compare the relative potency of sACE2(WT) sEVs with recombinant human ACE2 (rhACE2) in neutralizing the virus, we used Delta variant pseudovirus. sACE2(WT) sEVs blocked pseudovirus infection in a concentration-dependent manner and showed about 40% inhibition at 100 μg/ml containing 9.23 ng/ml of ACE2 whereas rhACE2 show less potency when an equivalent amount of ACE2 within sACE2(WT) sEVs was used, indicating that sEVs-mediated protein delivery conferred more superior activity than recombinant protein (Figure S3b, Supporting Information). Taken together, these results demonstrate that sEVs engineered to display sACE2 and its variants exhibited cross-reactive neutralization against WT and mutant S protein pseudotyped virus.

2.4 | Protection against authentic wildtype SARS-CoV-2 and Delta variant infection

To confirm the ability of sACE2 sEVs to suppress SARS-CoV-2 infectivity, we infected Vero E6 cells with Beta-CoV/Korea/KCDC03/2020 virus with or without sEVs. 0.01 MOI of the virus was mixed with sEVs and incubated with the cells. The cytopathic effects (CPEs) of SARS-CoV-2 on Vero E6 cells were determined using crystal violet staining. Normal staining, consistent with that in the non-infection and remdesivir (REM)-treated groups, was observed when sACE2.v1 sEVs and sACE2.v2 sEVs were incubated with the virus at 600 μg/ml. sACE2.v1 sEVs and sACE2.v2 sEVs exhibited inhibitory activity against SARS-CoV-2 even at a concentration of 100 μg/ml, whereas sACE2(WT) sEVs partially inhibited SARS-CoV-2 infectivity at the highest dose (Figure S4a, Supporting Information). qRT-PCR analysis of the viral E gene revealed that viral copy numbers were markedly decreased in the sACE2.v1 EV and sACE2.v2 EV-treated culture medium, whereas viral copy numbers, were only slightly altered by sACE2(WT) sEVs at 600 μg/ml. Moreover, the viral E gene was not detected in two out of four replicates of sACE2.v1 EV and sACE2.v2 EV treated at 100 μg/ml (Figure S4b, Supporting Information). These results confirmed the potent protective effects of sACE2.v1 sEVs and sACE2.v2 sEVs against authentic SARS-CoV-2 infection in Vero E6 cells. We also evaluated the sensitivity of the Delta variant to engineered sEVs. Surprisingly, immunostaining of SARS-CoV-2 N protein revealed that sACE2.v1 sEVs and sACE2.v2 sEVs potently blocked Delta variant infectivity at all concentrations. Moreover, even sACE2(WT) sEVs inhibited Delta variant infection in a concentration-dependent manner, whereas it only partially blocked wildtype SARS-CoV-2 at the highest dose (Figure 5a,b). Collectively, these findings demonstrated the high efficacy of engineered sACE2 sEVs in the inhibition of wildtype and Delta variant SARS-CoV-2 infection.

2.5 | Protection against SARS-CoV-2 infection in K18-hACE2 mice

To assess the efficacy of the engineered sEVs against the SARS-CoV-2 infection in vivo, we used K18-hACE2 transgenic mice expressing human ACE2 under cytokeratin 18 gene promoter (McCray et al., 2007). Due to the best efficacy of sACE2.v1 sEVs shown in vitro study, we chose to give K18-hACE2 mice a 200-μg dose of the sACE2.v1 sEVs by intraperitoneal injection once a day for 6 days after intranasal inoculation with SARS-CoV-2 (BetaCoV/Korea/KCDC03/2020) (Figure 6a). Compared to a PBS control mice, sACE2.v1 sEVs exhibited protection against SARS-CoV-2-induced weight loss and viral burden in the lungs of K18-hACE2 mice at 3 days after infection (Figure 6b,c; Figure S5a,b, Supporting Information). Furthermore, we observed significantly reduced induction of pro-inflammatory responses such as *Ifih1*, *Isg15*, and *Cxcl10* (Figure 6d). In conclusion, sACE2-engineered sEVs conferred protection against SARS-CoV-2 infection in vivo.

3 | DISCUSSION

An increasing number of studies have utilized sEVs for the effective delivery of diverse cargos, including proteins, DNA, mRNA, non-coding RNA, and lipids, to target organs (Liang et al., 2021). The presentation of specific proteins on the sEVs surface has allowed for functional protein delivery with broad applications. ACE2- and TMPRSS2-overexpressing sEVs were previously purified from 293FT cells and were shown to reduce the infectivity of SARS-CoV-2 S containing lentivirus (Cocozza et al., 2020). Further, ACE2-positive sEVs isolated from plasma inhibited RBD-binding to stably overexpressed ACE2 on cells (El-Shennawy et al.). While the current findings cannot be directly compared to these published data, sACE2(WT) sEVs exhibited marginal effects when compared to the effects described in previous reports. The neck domain, which is absent in sACE2, mediates ACE2 homodimerization to accommodate S trimer binding, which may partially explain the limited efficacy of sACE2(WT) sEVs (Barros et al., 2021; Yan et al., 2020). Nevertheless, the use of sACE2 variants optimized to bind the S protein on sEVs overcame this
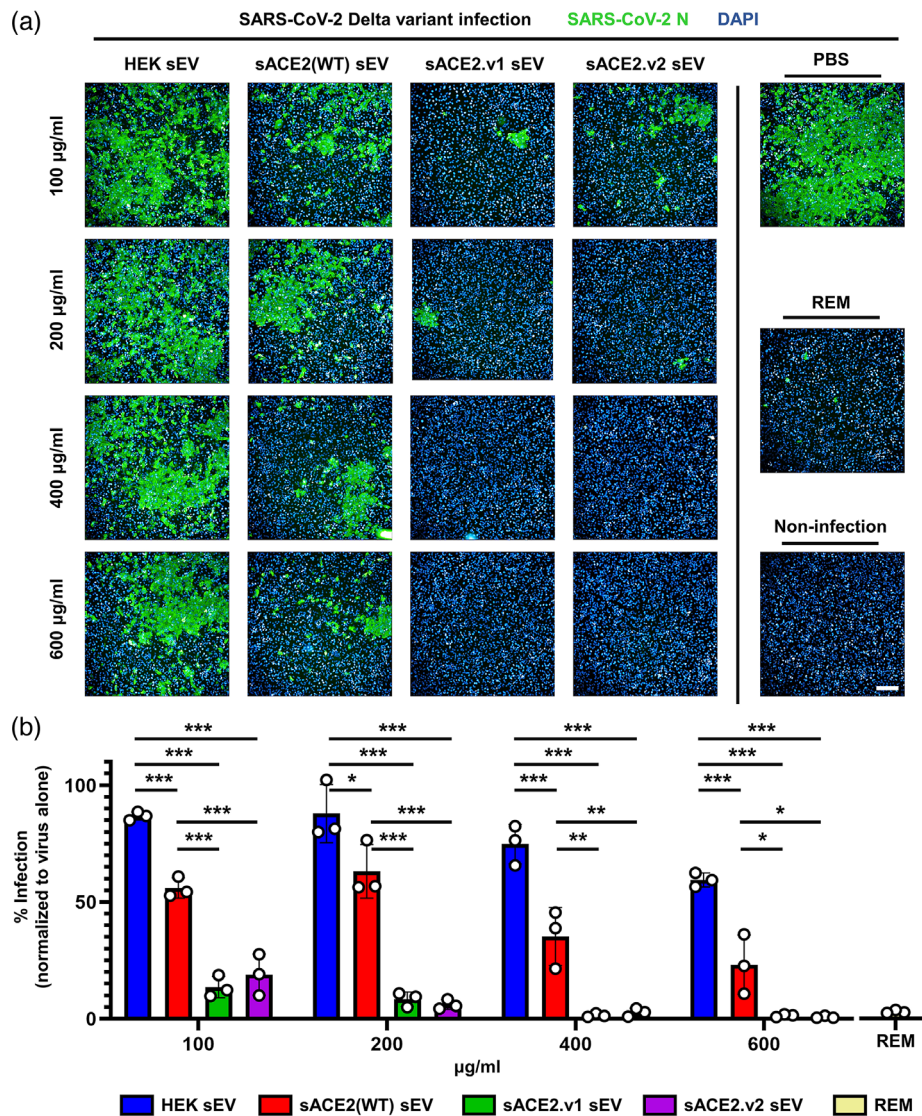
FIGURE 5 Protection against authentic Delta variant SARS-CoV-2 infection. (a) The immunostaining assays against SARS-CoV-2 N protein and DAPI for the Vero E6 cells infected by hCoV-19/South Korea/KDCA5439/2021. Remdesivir (REM) was used as positive control. (b) The infectivity of Delta variant was assessed using the ratio of N protein-positive cells to the total number of DAPI-stained cell nuclei. Values are normalized to virus alone (100%) ($n = 3$). Scale bars, 200 μm. *$P < 0.05$; **$P < 0.01$; ***$P < 0.001$ (one-way ANOVA with Tukey's multiple comparisons test)

limitation and allowed us to observe the significant efficacy of sACE2.v1 and sACE2.v2 sEVs. Further, D614G S-containing pseudovirus and RBD triple-mutant S-containing pseudovirus exhibited reduced infectivity in the presence of sACE2-loaded sEVs, indicating that accumulated escape mutations of the S protein, which augmented its affinity for ACE2, failed to compromise the efficacy of ACE2-targeting therapeutics (Chan et al., 2020). Of note, the approach of viral receptor display on sEVs for neutralization can be applied in the study of other viral infections, with examples including soluble DPP4-expressing sEVs for MERS-CoV and sialic acid-containing receptor-expressing sEVs for influenza virus (Moscona, 2005; Wang et al., 2013). Thus, the method described herein may have further applications for different viral diseases in the future.

A limitation of the current study is that we did not provide the mechanisms by which the sACE2-loaded sEVs showed better efficacy than recombinant sACE2 protein in neutralizing virus. However, it is expected that sACE2 sEVs should exert superior potency relative to recombinant sACE2 based on available literature. One study showed that sEVs expressing IL-12 on PTGFRN scaffolds exhibited more potent antitumor effects than recombinant IL-12, utilizing a similar EV surface display technique (Lewis et al., 2020). Another study revealed that exosomal ACE2 had superior neutralization efficacy against S-containing pseudovirus when compared with recombinant human ACE2 (El-Shennawy et al., 2020.). Due to their lipophilic nature and excellent stability, sEVs not only circulate in the blood but are also able to reach different cell populations, indicative of their potential for targeting specific cells, which, in conjunction with their longer half-life, would allow for greater in vivo efficacy compared to native recombinant protein (Zhao et al., 2020). Another limitation of the current study is that the pseudovirus used herein did not
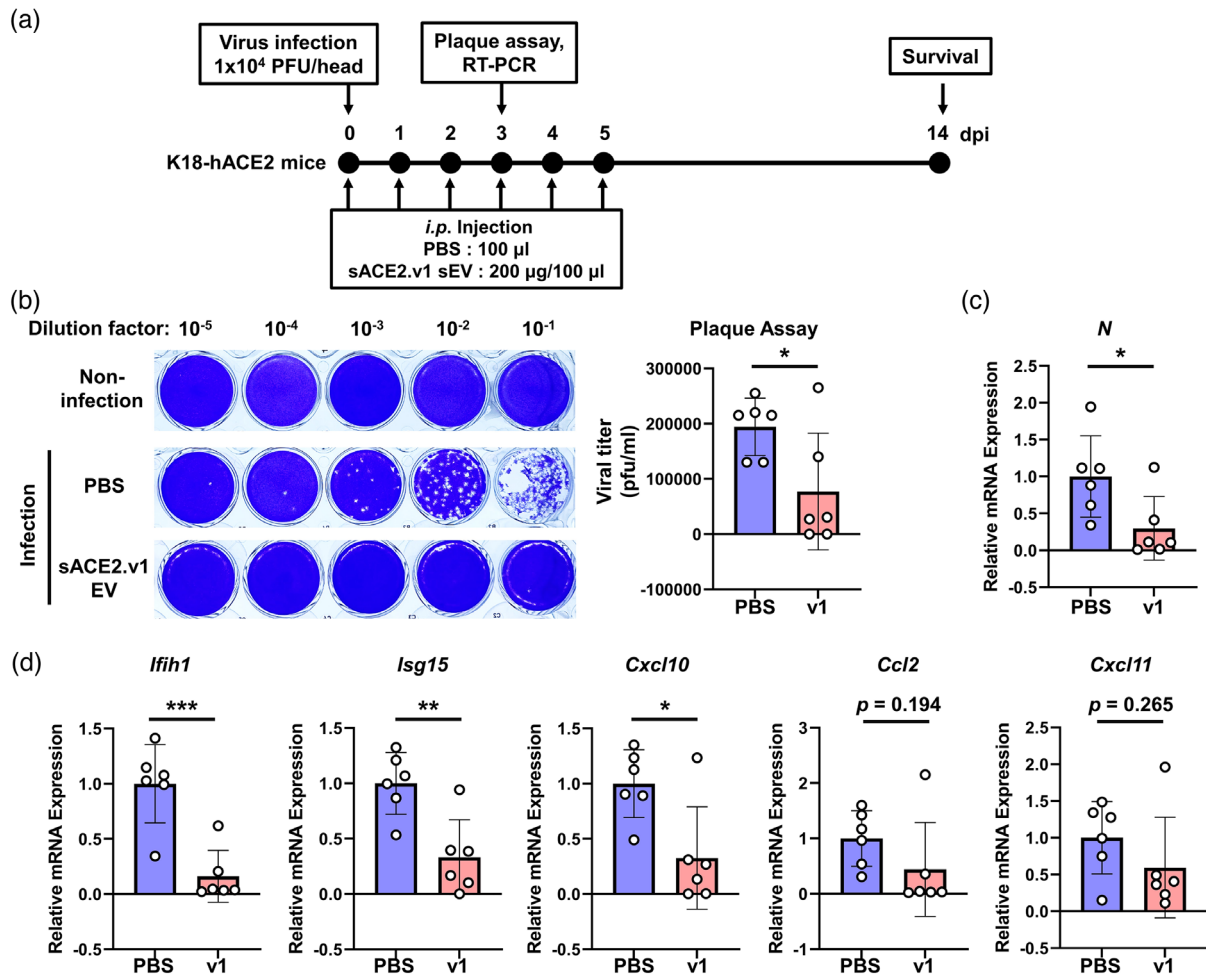
FIGURE 6 Anti-SARS-CoV-2 activities of sACE2.v1 sEVs in K18-hACE2 mice. (a) Schematic illustration of experimental design for K18-hACE2 mice infected with SARS-CoV-2. (b) K18-hACE2 mice were sacrificed at 3 days post infection (DPI) and viral titres in lungs were determined by plaque assay. Representative images of plaque assay and viral burden in the lungs ($n = 6$). (c) Viral RNA levels in the lungs at 3 DPI, as measure by qRT-PCR. (d) qRT-PCR analysis of expression in the lung homogenates of SARS-CoV-2-infected K18-hACE2 mice treated with PBS or sACE2.v1 sEVs. *$P < 0.05$; **$P < 0.01$; ***$P < 0.001$ (unpaired Student's t-test)

include the whole set of S mutations observed in Beta and Delta variants. Assessing the infectivity of authentic SARS-CoV-2 variants B.1.351 as well as other variants, such as B.1.1.7 and B.1.1.248 in vivo, will help recapitulate the infection observed in humans.

sEVs engineering allows for displaying native proteins on the sEVs surface, with various potential therapeutic applications. Herein, we showed that CD9ΔTM4 scaffolds successfully presented sACE2 and its variants on the sEVs surface. These sEVs inhibited binding between S and ACE2 in a dose-dependent manner by occupying available S protein as decoys. The infectivity of WT, D614G, Beta variant, and Delta variant mutant S-containing pseudovirus was compromised by sACE2.v1 and sACE2.v2 sEVs. Furthermore, both sEVs potently blocked authentic SARS-CoV-2 (BetaCoV/Korea/KCDC03/2020 virus) and Delta variant infection in Vero E6 cells. Furthermore, these inhibitory potencies of sACE2.v1 sEVs were confirmed in K18-hACE2 mice challenging SARS-CoV-2. Our observation that sACE2-expressing sEVs markedly protected against S-containing pseudovirus and authentic SARC-CoV-2 infection further supports the potential of engineered sEVs as an efficient platform for the delivery of therapeutics.

4 | MATERIALS AND METHODS

4.1 | Plasmid construction

To generate pCMV14-CD9ΔTM4-sACE2(WT)-3xFlag, pCMV14-CD9ΔTM4-sACE2.v1-3xFlag, and pCMV14-CD9ΔTM4-sACE2.v2-3xFlag construct, CD9ΔTM4 was first PCR-amplified from mEmerald-CD9-10 (Addgene, #54029) and subcloned

into a pCMV14-3xFlag vector (Sigma-Aldrich). For efficient cargo protein substitution, a KpnI restriction enzyme site was inserted in the linker between CD9ΔTM4 and sACE2. sACE2(WT), sACE2v1, and sACE2v2 were PCR-amplified from pcDNA3-sACE2(WT) (Addgene, #145147), pcDNA3-sACE2v1 (Addgene, #145148), and pcDNA3-sACE2v2 (Addgene, #145149), respectively. The obtained fragments were inserted into pCMV14-CD9ΔTM4-3xFlag using KpnI and XbaI restriction enzymes. To generate pCMV14-eGFP-CD9ΔTM4-sACE2, overlap extension PCR was performed as previously described (Hilgarth & Lanigan, 2020). Briefly, an eGFP fragment and CD9ΔTM4-sACE2 were PCR-amplified from pDONOR-tagBFP-PSM-EGFP (Addgene, #100603) and pCMV14-CD9ΔTM4-sACE2(WT), respectively. Overlap PCR was then performed using the primary fragments. Finally, fragments were subcloned into a pCMV14 vector between the NotI and XbaI sites. To generate the pLenti-hACE2-TagBFP construct, hACE2 and TagBFP were first PCR-amplified from hACE2 (Addgene, #1786), and pDONOR-tagBFP-PSM-EGFP, respectively, followed by overlap PCR of the primary fragments. The final PCR products were inserted into a pLenti-puro vector (Addgene, #39481) using XbaI and AgeI restriction enzymes. To produce pCMV14-SPIKE-TagBFP, each PCR-amplified primary fragment was used for overlap PCR. The final PCR products were inserted into the pCMV14 vector between the EcoRI and XbaI sites. To generate the pLenti-Luciferase-puro construct, luciferase was PCR-amplified from a pGL3-Basic vector (Promega) and subcloned into the pLenti-puro vector using BamHI and EcoRI restriction enzymes. To remove the endoplasmic reticulum (ER) retrieval signal at the C-terminal of the S protein, we generated pCMV14-Spike-dER constructs lacking the 30 C-terminal amino acids from pcDNA3.1-SARS2-Spike (#145032) via PCR (Ou et al., 2020). The amplified fragment was subcloned into a pCMV14-3xFlag vector. We generated the D614G mutant, the RBD mutations in Beta variant (K417N, E484K, and N501Y), mutations in Delta variant (L452R, E484K, and D614G) via site-directed mutagenesis as previously described (Liu & Naismith, 2008). To generate pCMV14-hACE2-3xFlag, hACE2 were PCR-amplified from hACE2 (Addgene, #1786). Subsequently, the PCR products were inserted into a pCMV14-3xFlag vector.

4.2 | Isolation and characterization of sEVs

To prepare conditioned media for sEVs isolation, we collected cell culture medium after transfection with 10 μg of plasmid DNA encoding CD9ΔTM4-sACE2(WT), v1, and v2. We replaced it with a serum-free medium. Isolation of sEVs from conditioned media (800 ml) was performed as previously described (Jung et al., 2020; Lee et al., 2021; Woo et al., 2020). Briefly, we centrifuged the collected medium at 800 g for 10 min to eliminate cellular debris, followed by filtering the resulting supernatant using a 70 μm strainer (Falcon) and a 0.22 μm bottle top filter (Merck Millipore). A tangential flow filtration (TFF) system with a 300-kDa MWCO (molecular weight cutoff) ultrafiltration membrane filter capsule (Pall Corporation) was used to isolate sEVs. We assessed sEVs protein concentration using a micro bicinchoninic acid (BCA) protein assay kit (Thermo Fisher Scientific). The amount and size distribution of sEVs were determined via nanoparticle tracking analysis (Malvern). Briefly, the camera level was set at 16, slide shutter of 1500, and analysis detection threshold of five. Three videos were recorded for a duration of 30 s. Isolated sEVs were in a final volume of approximately 5 ml. After purification, the sEVs were immediately stored in -70 °C freezers until use. The sEVs markers are analysed using CD63 antibody-coated magnetic microbeads (Immunostep). 40 μg of sEVs were incubated with microbeads overnight at room temperature. sEVs were washed and incubated with a biotinylated anti-CD81 antibody (Immunostep) for 1 h at 4°C. After being washed with wash buffer, sEVs were incubated with streptavidin-PE (Immunostep) for 30 min at 4°C. Later, 5000 microbeads were immediately analysed using BD FACS AriaIII (BD Biosciences) at the BIORP of Korea Basic Science Institute (KBSI). Beads were visualized by confocal laser scanning microscopy (Zeiss). The data were processed using FlowJo software.

4.3 | Cell culture and generation of stably transfected cell lines

HEK293T cells were purchased from ATCC and cultured in Dulbecco's Minimum Eagle's Medium (DMEM) (Capricorn) supplemented with 10% (v/v) foetal bovine serum(FBS; Gibco) and 1% (v/v) penicillin/streptomycin (Capricorn). Vero E6 cells were purchased from the ATCC and cultured in DMEM (Gibco) supplemented with 2 (infection media) or 10% (growth media) v/v heat-inactivated FBS and 1% v/v penicillin/streptomycin (Gibco). HEK293T cells stably expressing human ACE2-TagBFP (HEK293T-hACE2-TagBFP) were generated using lentiviral vectors comprising a CMV promoter and human ACE2 cDNA-Linker-TagBFP. Lentiviral particles (Lv-hACE2-TagBFP) were packaged, and HEK293T cells were transduced with Lv-hACE2-TagBFP. Puromycin selection (2 μg/ml) started 24 h after infection and continued for 14 days. hACE2-TagBFP-expressing cells were then purified using BD FACS AriaIII (BD Biosciences) at the BIORP of Korea Basic Science Institute (KBSI). HEK293T-hACE2-TagBFP cells were assayed as a polyclonal population. These cells were incubated in a humidified incubator at 5% $CO2$ at 37 °C. Cellular and sEVs fluorescence intensity was analysed using Cytation 5 Cell Imaging Multi-Mode Reader (BioTek).

4.4 | sEVs neutralization assay and authentic wildtype SARS-CoV-2 infection

BetaCoV/Korea/KCDC03/2020 (GISAID accession ID:EPI_ISL_407193) was obtained from the National Culture Collection for Pathogens of Korea Centre for Disease Control and Prevention Agency (KDCA) (Kim et al., 2020). Four concentrations of sEVs (600, 400, 200, and 100 μg/ml) were diluted in infection media to 2X assay concentration. An equal volume of media containing 200 pfu (0.01 multiplicity of infection (MOI)/well) of the virus was mixed with the sEVs and incubated for 1 h at 37°C. Following incubation, the mixture was added onto confluent Vero E6 cells (4×10^4 cells/well) in a 96-well plate for 1 h to allow infection. The mixture was removed, and the cells were washed twice with phosphate-buffered saline (PBS; Gibco), followed by incubation in fresh infection media for 72 h. Authentic virus infection was performed in biosafety level 3 facilities as per KDCA guidelines.

4.5 | Total RNA isolation, qRT-PCR, and CPE observations

For the quantification of viral copy number, total RNA was isolated from cell supernatants using the QIAamp 96 virus QIAcube HT kit (Qiagen) on a QIAcube HT system (Qiagen), according to the manufacturer's instructions. qRT-PCR was performed using the PowerCheck 2019-nCoV Real-time PCR kit (Kogene Biotech) and 7500 Real-time Fast Real-time PCR (Applied Biosystems) as follows: reverse transcription for 30 min at 50°C, initial denaturation for 10 min at 95 °C, and 40 cycles of denaturation for 15 s at 95 °C followed by an extension step of 1 min at 60 °C with primer/probe mix 1 (E gene) (Petrovan et al., 2020; Sung et al., 2020). The copy number was calculated based on the positive control (E gene).

For cytopathic effect (CPE) observation, the cells were fixed with 4% paraformaldehyde (Thermo Fisher Scientific) for 6 h and then stained with 1% crystal violet (Sigma-Aldrich) overnight.

4.6 | sEVs neutralization assay and authentic Delta variant SARS-CoV-2 infection

Four concentrations of sEVs (600, 400, 200, and 100 μg/ml) were diluted in infection media to 2X assay concentration. An equal volume of media containing 1,500 pfu (0.1 multiplicity of infection (MOI)/well) of hCoV-19/South Korea/KDCA5439/2021 (B.1.617.2) was mixed with the sEVs and incubated for 1 h at 37°C. Following incubation, the mixture was added onto confluent VeroE6 cells (1.5×10^4 cells/well) in a cell carrier ultra-96 plate (PerkinElmer) for 1 h to allow infection. The mixture was removed and the cells were washed twice with phosphate-buffered saline (PBS, Gibco) and incubated in fresh infection media for 24 h, and fixed with 4% formaldehyde for 15 min. Cells were washed and incubated for 2 h with anti-SARS-CoV-2 N antibody (1:2,000, Sinobio) in western blocking solution (Sigma-Aldrich) and then with Alexa488-conjugated rabbit antibody (1:2,000, Thermo Fisher Scientific) for 1 h. Subsequently, cells were incubated with DAPI (1:1,000, Abcam) in PBS for 10 min and washed five times with PBST (Sigma-Aldrich). Immunofluorescence images were acquired using a 10× objective with nine imaged fields per well by Operetta CLS (PerkinElmer). The acquired images were analysed using Harmony software (ver. 4.9, PerkinElemer) to quantify total cell numbers (nucleus numbers) and infected cell numbers. Infectivity of HEK sEVs, sACE2(WT) sEVs, sACE2(v1) sEVs, sACE2(v2) sEVs, and remdesivir (Medchemexpress) was normalized to virus alone (PBS) group.

4.7 | Mice

Female 6- to 8-week-old B6.Cg-Tg(K18-hACE2)2Prlmn/J mice purchased from the Jackson Laboratory were intranasally infected with 1×10^4 PFU of BetaCoV/Korea/KCDC03/2020 diluted in a total volume of 20 μl of PBS under anaesthesia. Subsequently, 200 μg of sACE.v1 sEVs diluted in a total volume of 100 μl of PBS or 100 μl of PBS were daily administered intraperitoneally for 6 days, starting from 1 h post-infection. Mouse survival and body weight changes were monitored until 14 days post-infection (DPI). On day 3 post-infection, six mice per group were euthanized, and the lungs were subjected to measure lung viral titres and expression levels of inflammatory cytokine genes. Mouse lungs were homogenized with Precellys Evolution (Bertin Corp.). Lung viral titres were determined by plaque assay, and inflammatory cytokine gene levels were assessed by qRT-PCR. Briefly, total RNA was isolated from mouse lungs using the Maxwell RSC viral total nucleic acid purification kit (Promega) by the Maxwell RSC 48 (Promega). Total RNA was reverse transcribed using PrimeScript RT reagent Kit with gDNA Eraser (Takara) and qRT-PCR was performed using TB Green Premix Ex Taq II (Takara). The primers used for qRT-PCR were listed in Table S1. The reference gene GAPDH was used as an internal standard for normalization. All mouse experiments were performed according to institutional guidelines of the KDCA (KDCA-IACUC-21-032) in animal biosafety level 3 facilities.

4.8 | Plaque assay (lung virus titre measurement)

Monolayers of Vero-E6 cells were prepared in 24-well plates. The cells were infected with tenfold serial dilutions of supernatant from homogenized mouse lung and incubated at 37°C for 1 h. The media was removed, and cells were washed with PBS. Each well was overlaid with MEM/agarose (Gibco) and maintained at room temperature until the overlay turned solid. Subsequently, the plates were incubated at 37°C for 72 h. The cells were then fixed with 4% paraformaldehyde (Thermo Fisher Scientific) and stained with 1% crystal violet (Sigma-Aldrich) overnight.

4.9 | Western blotting

The protein samples were prepared based on the previously described procedure (Park et al., 2021). Total protein was extracted from cells using a tissue protein extraction buffer mixture (Thermo Fisher Scientific) containing a protease inhibitor cocktail and a phosphatase inhibitor cocktail (Biovision). Protein concentrations were analysed using a BCA protein assay kit (Thermo Fisher Scientific). Lysates were mixed with NuPAGE LDS sample buffer (Thermo Fisher Scientific) with 5% β-mercaptoethanol. In the case of western blot for CD63, β-mercaptoethanol was not used. Proteins were separated via SDS-PAGE (Bio-rad) and transferred onto PVDF membranes (Merck Millipore). Primary antibodies used include anti-Flag (Sigma-Aldrich), anti-ACE2 (CST), anti-Calnexin (Merck Millipore), anti-tRFP (Evrogen), anti-TSG101 (Santa Cruz), anti-Alix (Santa Cruz), anti-CD9 (CST), anti-CD63 (Santa Cruz), anti-GM130 (CST) and anti-beta-actin (Sigma-Aldrich). Membranes were washed and incubated with peroxidase-conjugated anti-rabbit or anti-mouse secondary antibodies (Merck Millipore) for 1 h at room temperature. The immunoreactive protein bands were visualized using a Dyne ECL STAR Western Blot Detection Kit (Dyne Bio).

4.10 | ACE2/SARS-CoV-2 Spike S1 inhibitor screening assay

We tested engineered sEVs using the ACE2:Spike S1-Biotin (SARS-CoV-2) Inhibitor Screening Assay kit (BPS Bioscience) according to the manufacturer's instructions, with minor modifications. Briefly, instead of incubation on an ACE2-coated plate, sEVs were incubated with S1-biotin protein for 1 h at room temperature with slow shaking. Thereafter, the sEVs and S1-biotin mixture were added onto an ACE2-coated plate and incubated for another hour. The rest of the procedures were performed according to the manufacturer's protocol.

4.11 | Generation of pseudovirus and lentivirus

S-containing SARS-CoV-2 pseudotyped lentivirus was produced as previously described (Nie et al., 2020). Briefly, HEK293T cells were transfected with 2 μg of pLenti-Luciferase, 7.5 μg of pRSV-Rev (Addgene, #12253), 7.5 μg of pMDLg/pRRE (Addgene, #12251) and 5 μg of pCMV14-Spike-ΔER using polyethylenimine (PEI) reagent (Sigma-Aldrich). Cells were incubated with full medium (DMEM+10% heat-inactivated FBS+1% penicillin/streptomycin). On the following day, the medium was replaced with a full medium containing 25 mM HEPES. After 48 h, the supernatant was centrifuged for 10 min at 800 g to remove the dead cells and passed through a 0.45 μm syringe filter (Advantec). The filtrates were concentrated with Lenti-X Concentrator (Takara) according to the manufacturer's protocol. Lentivirus was packaged by transfecting HEK293T cells with 2 μg of pLenti-hACE2-TagBFP, 7.5 μg of pRSV-Rev, 7.5 μg of pMDLg/pRRE, and 5 μg of pMD2.G (Addgene, #12259) using PEI.

4.12 | Luciferase assay

S pseudotyped virus was incubated with sACE2(WT) sEVs, sACE2v1 sEVs, sACE2v2 sEVs or normal HEK293T sEVs in full medium containing polybrene (10 μg/ml) for 1 h at room temperature. HEK293T-hACE2-TagBFP cells plated in a 24-well tissue culture plate were then infected with the sEVs-incubated pseudotyped virus. On the following day, the medium was replaced with full medium. After 48h, cells were lysed in passive lysis buffer (Promega) and luciferase activity was measured using a Luciferase Assay System (Promega) with a luminometer (Berthold) to assess viral infectivity. Recombinant human ACE2 protein (His Tag) was purchased from Sino Biological.

4.13 | Transmission electron microscopy

For cryo TEM, sEVs were collected on a lacey carbon grid (Electron Microscopy Sciences). The grids were frozen in liquid nitrogen. Images were obtained using the Tecnai Twin transmission electron microscope at 200 kV.

4.14 | Immunoprecipitation

HEK293T cells were transiently transfected with pCMV14 or pCMV14-SPIKE-TagBFP and then lysed with lysis buffer [20 mM HEPES pH 7.4, 0.5 mM EDTA, 150 mM NaCl, 1% Triton X-100 containing protease inhibitors]. Immunoprecipitation was performed using SureBeads™ Protein A Magnetic Beads (Bio-rad) and an anti-tRFP antibody (Evrogen) according to the manufacturer's protocol, with minor modifications. Before elution with LDS sample buffer (Thermo Fisher Scientific), bead-bound S-TagBFP was incubated with sEVs overnight. sEVs were washed with PBS three times and then eluted with sample buffer.

4.15 | ACE2 ELISA

The concentrations of human sACE2 in sEVs were determined with ELISA kits purchased from Aviscera Bioscience. ELISA was performed according to the manufacturer's instructions. The optical density of each well was determined using a microplate reader set to 450 nm (Biotek).

4.16 | Data analysis

All statistical analyses were performed with Prism9 (Graphpad Software) using one-way ANOVA with Tukey's multiple comparisons test for comparing more than three samples. Unpaired Student's t-test were used to test significance between two samples. Data are presented as the mean $\pm$ s.d. Groups were considered significantly different when $P < 0.05$ (*$P < 0.05$; **$P < 0.01$; ***$P < 0.001$).

CONFLICT OF INTEREST
Y.W.C. is the chief executive officer of ExoStemTech Inc. D.-G.J. and J.H.P. are stockholders of ExoStemTech Inc. H.K.K, E.K., J.K., Y.W.C., D.-G.J. have filed a patent application based on this work.

ORCID
Dong-Gyu Jo 🆔 https://orcid.org/0000-0003-2271-1076

REFERENCES
Barros, E. P., Casalino, L., Gaieb, Z., Dommer, A. C., Wang, Y., Fallon, L., Raguette, L., Belfon, K., Simmerling, C., & Amaro, R. E. (2021). The flexibility of ACE2 in the context of SARS-CoV-2 infection. *Biophysical Journal* 120, 1072–1084.

Böker, K. O., Lemus-Diaz, N., Rinaldi Ferreira, R., Schiller, L., Schneider, S., & Gruber, J. (2018). The Impact of the CD9 Tetraspanin on Lentivirus Infectivity and Exosome Secretion. *Molecular Therapy : The Journal of the American Society of Gene Therapy*, 26, 634–647.

Boucheix, C., Benoit, P., Frachet, P., Billard, M., Worthington, R. E., Gagnon, J., & Uzan, G. (1991). Molecular cloning of the CD9 antigen. A new family of cell surface proteins. *The Journal of Biological Chemistry*, 266, 117–122.

Chan, K. K., Dorosky, D., Sharma, P., Abbasi, S. A., Dye, J. M., Kranz, D. M., Herbert, A. S., & Procko, E. (2020). Engineering human ACE2 to optimize binding to the spike protein of SARS coronavirus 2. *Science*, 369, 1261–1265.

Cocozza, F., Névo, N., Piovesana, E., Lahaye, X., Buchrieser, J., Schwartz, O., Manel, N., Tkach, M., Théry, C., & Martin-Jaular, L. (2020). Extracellular vesicles containing ACE2 efficiently prevent infection by SARS-CoV-2 Spike protein-containing virus. *Journal of Extracellular Vesicles*, 10, e12050.

Duong, N., Curley, K., Brown, A., Campanelli, A., Do, M. A., Levy, D., Tantry, A., Marriott, G., & Lu, B. (2019). Decoy exosomes as a novel biologic reagent to antagonize inflammation. *International Journal of Nanomedicine*, 14, 3413–3425.

El-Shennawy, L., Hoffmann, A. D., Dashzeveg, N. K., Mehl, P. J., Yu, Z., Tokars, V. L., Nicolaescu, V., Ostiguin, C., Jia, Y., Li, L., et (2020). Circulating ACE2-expressing exosomes block SARS-CoV-2 infection as an innate antiviral mechanism. *BioRxiv*,.

Hilgarth, R. S., & Lanigan, T. M. (2020). Optimization of overlap extension PCR for efficient transgene construction. *MethodsX*, 7, 100759.

Hoffmann, M., Kleine-Weber, H., Schroeder, S., Krüger, N., Herrler, T., Erichsen, S., Schiergens, T. S., Herrler, G., Wu, N.-H., Nitsche, A., Müller, M. A., Drosten, C., & Pöhlmann, S. (2020). SARS-CoV-2 cell entry depends on ACE2 and TMPRSS2 and is blocked by a clinically proven protease inhibitor. *Cell*, *181*, 271-280.e8.

Hu, J., Peng, P., Wang, K., Fang, L., Luo, F.-Y., Jin, A.-S., Liu, B.-Z., Tang, N., & Huang, A.-L. (2021). Emerging SARS-CoV-2 variants reduce neutralization sensitivity to convalescent sera and monoclonal antibodies. *Cellular & Molecular Immunology*, *18*, 1061–1063.

Jung, Y. J., Kim, H. K., Cho, Y., Choi, J. S., Woo, C. H., Lee, K. S., Sul, J. H., Lee, C. M., Han, J., Park, J. H., Jo, D.-G., & Cho, Y. W. (2020). Cell reprogramming using extracellular vesicles from differentiating stem cells into white/beige adipocytes. *Science Advances*, *6*, 6721.

Kim, J.-M., Chung, Y.-S., Jo, H. J., Lee, N.-J., Kim, M. S., Woo, S. H., Park, S., Kim, J. W., Kim, H. M., & Han, M.-G. (2020). Identification of coronavirus isolated from a patient in Korea with covid-19. *Osong Public Health and Research Perspectives*, *11*, 3–7.

Kourembanas, S. (2015). Exosomes: Vehicles of intercellular signaling, biomarkers, and vectors of cell therapy. *Annual Review of Physiology*, *77*, 13–27.

Lee, K. S., Lee, J., Kim, H. K., Yeom, S. H., Woo, C. H., Jung, Y. J., Yun, Y. E., Park, S. Y., Han, J., Kim, E., Sul, J. H., Jung, J. M., Park, J. H., Choi, J. S., Cho, Y. W., & Jo, D.-G. (2021). Extracellular vesicles from adipose tissue-derived stem cells alleviate osteoporosis through osteoprotegerin and miR-21-5p. *Journal of Extracellular Vesicles*, *10*, e12152.

Lei, C., Qian, K., Li, T., Zhang, S., Fu, W., Ding, M., & Hu, S. (2020). Neutralization of SARS-CoV-2 spike pseudotyped virus by recombinant ACE2-Ig. *Nature Communications*, *11*, 1–5.

Lewis, N. D., Sia, C. L., Kirwin, K., Haupt, S., Mahimkar, G., Zi, T., Xu, K., Dooley, K., Jang, S. C., Choi, B., Boutin, A., Grube, A., Mccoy, C., Sanchez-Salazar, J., Doherty, M., Gaidukov, L., Estes, S., Economides, K. D., Williams, D. E., & Sathyanarayanan, S. (2020). Exosome surface display of IL12 results in tumor-retained pharmacology with superior potency and limited systemic exposure compared with recombinant IL12. *Molecular Cancer Therapeutics*, *20*, 523–534.

Liang, Y., Duan, L., Lu, J., & Xia, J. (2021). Engineering exosomes for targeted drug delivery. *Theranostics*, *11*, 3183–3195.

Liu, H., & Naismith, J. H. (2008). An efficient one-step site-directed deletion, insertion, single and multiple-site plasmid mutagenesis protocol. *BMC Biotechnology [Electronic Resource]*, *8*, 91.

Madhi, S. A., Baillie, V., Cutland, C. L., Voysey, M., Koen, A. L., Fairlie, L., Padayachee, S. D., Dheda, K., Barnabas, S. L., Bhorat, Q. E., Briner, C., Kwatra, G., Ahmed, K., Aley, P., Bhikha, S., Bhiman, J. N., Bhorat, A. E., Du Plessis, J., Esmail, A., … Izu, A. (2021). Efficacy of the ChAdOx1 nCoV-19 Covid-19 vaccine against the B.1.351 variant. *New England Journal of Medicine*, *384*, 1885–1898.

Mccray, P. B., Pewe, L., Wohlford-Lenane, C., Hickey, M., Manzel, L., Shi, L., Netland, J., Jia, H. P., Halabi, C., Sigmund, C. D., Meyerholz, D. K., Kirby, P., Look, D. C., & Perlman, S. (2007). Lethal infection of K18- hACE2 mice infected with severe acute respiratory syndrome coronavirus. *Journal of Virology*, *81*, 813–821.

Monteil, V., Kwon, H., Prado, P., Hagelkrüys, A., Wimmer, R. A., Stahl, M., Leopoldi, A., Garreta, E., Hurtado Del Pozo, C., Prosper, F., Romero, J. P., Wirnsberger, G., Zhang, H., Slutsky, A. S., Conder, R., Montserrat, N., Mirazimi, A., & Penninger, J. M. (2020). Inhibition of SARS-CoV-2 infections in engineered human tissues using clinical-grade soluble human ACE2. *Cell*, *181*, 905-913.e7.e7.

Moscona, A. (2005). Neuraminidase Inhibitors for Influenza. *New England Journal of Medicine*, *353*, 1363–1373.

Nie, J., Li, Q., Wu, J., Zhao, C., Hao, H., Liu, H., Zhang, L., Nie, L., Qin, H., Wang, M., Lu, Q., Li, X., Sun, Q., Liu, J., Fan, C., Huang, W., Xu, M., & Wang, Y. (2020). Establishment and validation of a pseudovirus neutralization assay for SARS-CoV-2. *Emerging Microbes & Infections*, *9*, 680–686.

Ou, X., Liu, Y., Lei, X., Li, P., Mi, D., Ren, L., Guo, L., Guo, R., Chen, T., Hu, J., Xiang, Z., Mu, Z., Chen, X., Chen, J., Hu, K., Jin, Q., Wang, J., & Qian, Z. (2020). Characterization of spike glycoprotein of SARS-CoV-2 on virus entry and its immune cross-reactivity with SARS-CoV. *Nature Communications*, *11*, 1–12.

Park, J., Ha, H.-J., Chung, E. S., Baek, S. H., Cho, Y., Kim, H. K., Han, J., Sul, J. H., Lee, J., Kim, E., Kim, J., Yang, Y. R., Park, M., Kim, S. H., Arumugam, T. V., Jang, H., Seo, S. W., Suh, P.-G., & Jo, D.-G. (2021). O-GlcNAcylation ameliorates the pathological manifestations of Alzheimer's disease by inhibiting necroptosis. *Science Advances*, *7*, 1–18.

Petrovan, V., Vrajmasu, V., Bucur, A. C., Soare, D. S., Radu, E., Dimon, P., & Zaulet, M. (2020). Evaluation of commercial qPCR kits for detection of SARS-CoV-2 in pooled samples. *Diagnostics*, *10*, 472.

Planas, D., Veyer, D., Baidaliuk, A., Staropoli, I., Guivel-Benhassine, F., Rajah, M. M., Planchais, C., Porrot, F., Robillard, N., Puech, J., Prot, M., Gallais, F., Gantner, P., Velay, A., Le Guen, J., Kassis-Chikhani, N., Edriss, D., Belec, L., Seve, A., … Schwartz, O. (2021). Reduced sensitivity of SARS-CoV-2 variant Delta to antibody neutralization. *Nature*, *596*, 276–280.

Plante, J. A., Liu, Y., Liu, J., Xia, H., Johnson, B. A., Lokugamage, K. G., Zhang, X., Muruato, A. E., Zou, J., Fontes-Garfias, C. R., Mirchandani, D., Scharton, D., Bilello, J. P., Ku, Z., An, Z., Kalveram, B., Freiberg, A. N., Menachery, V. D., Xie, X., … Shi, P.-Y. (2021). Spike mutation D614G alters SARS-CoV-2 fitness. *Nature*, *592*, 116–121.

Sung, H., Roh, K. H., Hong, K. H., Seong, M.-W., Ryoo, N., Kim, H. S., Lee, J., Kim, S. Y., Yoo, S., Kim, M.-N., Han, M. G., Lee, S. W., Lee, H., & Yoo, C. K. (2020). COVID-19 molecular testing in Korea: Practical essentials and answers from experts based on experiences of emergency use authorization assays. *Annals of Laboratory Medicine*, *40*, 439–447.

Théry, C., Witwer, K. W., Aikawa, E., Alcaraz, M. J., Anderson, J. D., Andriantsitohaina, R., Antoniou, A., Arab, T., Archer, F., Atkin-Smith, G. K., Ayre, D. C., Bach, J.-M., Bachurski, D., Baharvand, H., Balaj, L., Baldacchino, S., Bauer, N. N., Baxter, A. A., Bebawy, M., … Zuba-Surma, E. K. (2018). Minimal information for studies of extracellular vesicles 2018 (MISEV2018): a position statement of the International Society for Extracellular Vesicles and update of the MISEV2014 guidelines. *Journal of Extracellular Vesicles*, *7*, 1535750.

Wang, N., Shi, X., Jiang, L., Zhang, S., Wang, D., Tong, P., Guo, D., Fu, L., Cui, Y., Liu, X., Arledge, K. C., Chen, Y.-H., Zhang, L., & Wang, X. (2013). Structure of MERS-CoV spike receptor-binding domain complexed with human receptor DPP4. *Cell Research*, *23*, 986–993.

Wibmer, C. K., Ayres, F., Hermanus, T., Madzivhandila, M., Kgagudi, P., Oosthuysen, B., Lambson, B. E., De Oliveira, T., Vermeulen, M., Van Der Berg, K., Rossouw, T., Boswell, M., Ueckermann, V., Meiring, S., Von Gottberg, A., Cohen, C., Morris, L., Bhiman, J. N., & Moore, P. L. (2021). SARS-CoV-2 501Y.V2 escapes neutralization by South African COVID-19 donor plasma. *Nature Medicine*, *27*, 622–625.

Woo, C. H., Kim, H. K., Jung, G. Y., Jung, Y. J., Lee, K. S., Yun, Y. E., Han, J., Lee, J., Kim, W. S., Choi, J. S., Yang, S., Park, J. H., Jo, D.-G., & Cho, Y. W. (2020). Small extracellular vesicles from human adipose-derived stem cells attenuate cartilage degeneration. *Journal of Extracellular Vesicles*, *9*, 1735249.

Wrapp, D., Wang, N., Corbett, K. S., Goldsmith, J. A., Hsieh, C.-L., Abiona, O., Graham, B. S., & Mclellan, J. S. (2020). Cryo-EM structure of the 2019-nCoV spike in the prefusion conformation. *Science*, *367*, 1260–1263.

Wu, J. T., Leung, K., & Leung, G. M. (2020). Nowcasting and forecasting the potential domestic and international spread of the 2019-nCoV outbreak originating in Wuhan, China: A modelling study. *Lancet*, *395*, 689–697.

Yan, R., Zhang, Y., Li, Y., Xia, L., Guo, Y., & Zhou, Q. (2020). Structural basis for the recognition of SARS-CoV-2 by full-length human ACE2. *Science*, *367*, 1444–1448.

Yim, N., Ryu, S.-W., Choi, K., Lee, K. R., Lee, S., Choi, H., Kim, J., Shaker, M. R., Sun, W., Park, J.-H., Kim, D., Heo, W. D., & Choi, C. (2016). Exosome engineering for efficient intracellular delivery of soluble proteins using optically reversible protein–protein interaction module. *Nature Communications*, *7*, 12277.

Zhao, X., Wu, D., Ma, X., Wang, J., Hou, W., & Zhang, W. (2020). Exosomes as drug carriers for cancer therapy and challenges regarding exosome uptake. *Biomedicine & Pharmacotherapy = Biomedecine & Pharmacotherapie*, *128*, 110237.

Zoufaly, A., Poglitsch, M., Aberle, J. H., Hoepler, W., Seitz, T., Traugott, M., Grieb, A., Pawelka, E., Laferl, H., Wenisch, C., Neuhold, S., Haider, D., Stiasny, K., Bergthaler, A., Puchhammer-Stoeckl, E., Mirazimi, A., Montserrat, N., Zhang, H., Slutsky, A. S., & Penninger, J. M. (2020). Human recombinant soluble ACE2 in severe COVID-19. *The lancet. Respiratory medicine*, *8*, 1154–1158.

SUPPORTING INFORMATION

Additional supporting information may be found in the online version of the article at the publisher's website.